Astron. Astrophys. 324, 490–504 (1997)

ASTRONOMY AND ASTROPHYSICS

The determination of the star formation rate in galaxies

G. Barbaro[1] **and B.M. Poggianti**[2,3,4]

[1] Dipartimento di Astronomia, vicolo dell'Osservatorio 5, I-35122 Padova, Italy (barbaro@astrpd.pd.astro.it)
[2] Institute of Astronomy, Madingley Road, Cambridge CB3 0HA, UK
[3] Royal Greenwich Observatory, Madingley Road, Cambridge CB3 0EZ, UK
[4] Kapteyn Instituut, P.O. Box 800, 9700 AV Groningen, The Netherlands (bianca@astro.rug.nl)

Received 25 July 1996 / Accepted 17 February 1997

Abstract. A spectrophotometric model able to compute the integrated spectrum of a galaxy, including the contribution both of the stellar populations and of the ionized interstellar gas of the HII regions powered by young hot stars, has been used to study several spectral features and photometric quantities in order to derive calibrations of the star formation history of late type galaxies. Attention has been paid to analyze the emission of the Balmer lines and the [OII]λ3727 line to test their attitude at providing estimates of the present star formation rate in galaxies. Other features, like D_{4000} and the equivalent width of the H_δ line, influenced by the presence of intermediate age stars, have been considered.

Several ways of estimating the star formation rates in normal galaxies are discussed and some considerations concerning the applicability of the models are presented. Criteria have been also studied for ascertaining the presence of a burst, current or ended not long ago. Bursts usually hinder the determination of the past star formation rate.

Key words: galaxies: evolution – galaxies: stellar content – galaxies: fundamental parameters – H II regions

1. Introduction

The star formation history is a fundamental quantity in the study of the galaxy populations and their evolution. It is becoming evident that this evolution can be influenced by the interactions with the intergalactic medium or with other galaxies, giving rise to episodes of intense star formation (bursts). Accordingly the elaboration of methods for evaluating the star formation rate (SFR) is one of the tasks of the research in this field.

Clearly the needed information arises from the integrated spectra and especially from spectral features contributed by stars or by the ionized interstellar gas. In this work we present an analysis of some of such features which are able to disclose the presence of stars of a given age and therefore can yield estimates of the SFR in different epochs of the galaxy life. To this aim we have developed a spectrophotometric model which takes into account both the stellar and the nebular contribution. The model predictions have been compared with a sample of observational data and from this comparison suitable quantities for the evaluation of the SFR have been singled out. Moreover criteria for ascertaining the occurrence of bursts, both current or recently concluded, have been derived.

The observational material consists of the sample of spectra of local galaxies of Kennicutt (1992a) including both normal galaxies, that is galaxies of the standard morphological sequence, and starburst galaxies. With such spectra, available in digital records from the Astronomical Data Center, Kennicutt's analysis has been extended by deriving other spectral features besides those computed by him. The comparison with the spectrophotometric model has allowed: a) to derive calibrations of the SFR in terms of several quantities, especially the intensities of the emission lines, b) to single out relations which are valid independently of the history of star formation of the galaxy, c) to find out quantities which can descriminate between normal and starburst galaxies.

The comparison with the spectra of normal galaxies allows to test the capability of the model to reproduce a large set of spectral features for all the galactic types. The model thus tested can be used generally in the study of distant galaxies in the frame of the problems of galaxy evolution.

2. The spectrophotometric model

The theoretical tool used is an evolutionary synthesis model able to compute the integrated spectrum of a galaxy from the far UV region up to the IR including both the contribution of the stellar component and the thermal emission of the gas in HII regions. The non-thermal gaseous emission, arising from non-stellar ionizing sources and important only in AGN, and the far IR emission of dust are not considered.

Send offprint requests to: G. Barbaro

2.1. The stellar spectrum

The emission of the stellar component is derived with an updated version of a previous model computed by Barbaro and Olivi (1986, 1989). It takes into account all the advanced evolutionary phases up to the AGB and post-AGB, while it does not consider the pre-main sequence, where the visible light of the most luminous stars is completely extincted or their contribution is negligible due to the small lifetime of this phase. The presence of populations of stars of different metallicity is envisaged, the chemical evolution being computed in a simple way. While the evolutionary background, which has been described in detail in Barbaro & Olivi (1989), has not been changed, substantial improvements have been introduced in the spectral library. First of all the new atmosphere models of Kurucz (in the 1993 version) have been adopted.

In the IR region atmosphere models of cool stars are not much reliable because of the uncertainties affecting the input of atomic and molecular data concerning the opacities. Therefore for stars with $T_{eff} < 5500$ K the library of observed spectra of Lançon - Rocca Volmerange (1992, LRV) has been adopted. This library covers the spectral interval 14500 - 25000 Å (and therefore includes the H and K bands of Johnson's photometric system) with a resolution of about 25 and 70 Å respectively at the lower and the upper end of the observed region. Although it includes stars with different metallicities, the small number of them prevents an organization in categories of different metal content and therefore a unique calibration independently of Z has been adopted. For stars with $T_{eff} > 5500$ K Kurucz's models have been used. The region of wavelengths higher than 25000 Å has not been included as it is heavily affected by the dust emission, which we have not considered. A crucial point is the fit of the visible and IR spectra: the fit has been performed with the aid of a black body spectrum. The difficult task is to determine its temperature due to the weak dependence on it of the spectrum at such wavelengths. We have adopted an iterative procedure by choosing a suitable temperature and using the corresponding black body as a fitting support; with the obtained spectrum broad band optical and IR colours have been obtained and compared with those observed for the same effective temperature (Koornneef 1983, Bessell & Brett 1988, LRV). The fitting temperature was changed until agreement between computed and observed colours was reached. Kurucz's models and observed spectra of LRV agree very well for early type and intermediate type stars and on this ground theoretical spectra have been used also for sufficiently hot stars. Systematic differences appear instead for later types, for which the computed (H-K) colour is bluer than the observed one.

Kurucz's models (1993) have been also used for the synthesis of the integrated spectra in the far UV region. From the spectral energy distributions in the UV region the flux of the ionizing photons has been derived in the computation of the nebular emission. The spectral distributions of stars hotter than 50000 K, not included in Kurucz's library, have been approximated with black body spectra.

Since the spectral resolution of Kurucz's atmosphere models does not allow the synthesis of some spectral features (e.g. the Balmer absorption lines) in the visible region, also the library of stellar spectra of Jacoby et al. (1984) has been used. The stars considered in this last catalogue cover all the spectral types from O to M, all the luminosity classes and have, with few exceptions, solar metallicity; their spectra, which have been corrected for interstellar reddening, have a resolution of about 4.5 Å. The link with the isochronous lines has been obtained with Schmidt-Kaler's T_e– Spectral Type relations, as presented in Tables 4.1.4.3 and 4.1.5.23 of Landolt - Börnstein (1982). In the common spectral interval both libraries give almost equal integrated continua of simple stellar populations and galaxies. Small differences appear when comparing spectra of metal–poor populations since, as already remarked, the spectra of Jacoby et al. (1984) have solar composition; however, as long as extreme situations are excluded, the results are very similar.

2.2. The ionized gas emission: the line spectrum

Models of HII regions excited by single stars of different effective temperature have been computed by several authors: in particular Rubin (1985) and Stasinska (1990) have investigated a variety of parameters (chemical composition and density of the gas, effective temperature and luminosity of the exciting stars). From the analysis of these models a relevant feature emerges: in models with different ionization parameter U the line fluxes do not scale with the flux of the ionizing photons. This implies that the emission of an HII region powered by a group of stars, all having the same temperature, cannot be computed from the models of an HII region powered by a single star having that temperature and luminosity equal to the sum of luminosities. Having in mind these circumstances let us examine the construction of the nebular spectrum of a galaxy. Let us assume that the nebular emission of the galaxy is the sum of the contributions of the HII regions excited by all the hot young stars. The integrated $H\beta$ luminosity, in the hypothesis that the HII regions are ionization-bound, is then given by:

$$L(H\beta) = \int\int B(m,t) l_{H\beta}(m,t) dm dt \qquad (1)$$

where $l_{H\beta}(m,t)$ is the $H\beta$ luminosity of a star of mass m born at time t. $B(m,t)$ is the distribution function of masses and birth times of the stars. In principle the integral should be extended to all the hot stars with a conspicuous UV flux, but in the case of late type galaxies, such as those of concern in the present work, the ionizing radiation due to the young massive stars is at least five order of magnitude larger than that originating from hot old stars (Binette et al. 1994). According to Osterbrock (1989), $l_{H\beta}(m,t)$ is given by:

$$l_{H\beta}(m,t) = h\nu_{H\beta} \frac{\alpha_{H\beta}}{\alpha_B} n_c(m,t) = K_{H\beta} n_c(m,t) \qquad (2)$$

where $h\nu_{H\beta}$ is the energy of photons with λ = 4862 Å, $\alpha_{H\beta}$ and α_B are respectively the coefficient of recombination with

emission of the $H\beta$ line and the total recombination coefficient (case B, optically thick). $K_{H\beta}$ is a function of the electron temperature which, to a first approximation, depends only on the chemical composition. n_c is the number of ionizing photons emitted per second from a star with mass m and age $\tau = T_G - t$, where T_G is the age of the galaxy. By keeping $K_{H\beta}$=constant, Eq. (1) becomes:

$$L(H_\beta) = K_{H\beta} \int\int B(m,t) n_c(m,t) dm dt = K_{H\beta} N_c \quad (3)$$

being N_c the integrated ionizing flux of the galaxy,

$$N_c = \int\int B(m,t) n_c(m,t) dm dt \quad (4)$$

Usually one sets: $B(m,t) = \psi(t)\phi(m)$ and therefore:

$$N_c = \int_{T-\tau_M}^{T} \psi(t) \mathscr{N}_c(T-t) dt \quad (5)$$

which is computed by considering only hot stars with $\tau \leq \tau_m = 4 \cdot 10^7$ yr; τ_M is the maximum age of a cluster still able to power a non negligible HII region. $\mathscr{N}_c(T-t)$ is the integrated UV flux of a generation born at the time t.

This procedure can be extended to a generic Balmer line H_ι and to any other hydrogen emission line since:

$$\frac{l_{H\iota}(m,t)}{l_{H\beta}(m,t)} = h_{H\iota} \quad (6)$$

(Osterbrock 1989) with $h_{H\iota}$ is function of the gas temperature alone. The independence of $l_{H\iota}/l_{H\beta}$ from m and t can be verified on Rubin's (1985) and Stasinska's models (1990). Therefore:

$$L(H_\iota) = h_{H\iota} \int\int B(m,t) l_{H\beta}(m,t) dm dt = h_{H\iota} K_{H\beta} N_c \quad (7)$$

The behaviour of the emission lines of elements other than hydrogen is different. Let us consider the line of the generic X element (such is for instance OII) at the wavelength λ. We then have:

$$L(X_\lambda) = \int\int B(m,t) l_{x_\lambda}(m,t) dm dt \quad (8)$$

with

$$\frac{l_{x_\lambda}(m,t)}{l_{H\beta}(m,t)} = h_{X_\lambda}(m,t) \quad (9)$$

According to the models of Rubin (1985) and Stasinska (1990) $l_{x_\lambda}/l_{H\beta}$ is really function not only of the effective temperature of the source of the ionizing photons but also of their luminosity and therefore of m and t, in the frame of the theories of stellar evolution. Therefore the line luminosity is given by

$$L(X_\lambda) = \int_{T-\tau_M}^{T} \psi(t) \mathscr{L}_{X_\lambda}(T-t) dt \quad (10)$$

where $\mathscr{L}_{X_\lambda}(T-t)$ is the contribution of all the stars born at the time t. No other simplification can be introduced.

We can therefore conclude that:

a) as far as the Balmer lines are concerned, by virtue of Eq. (3), a galaxy can be treated as a unique HII region powered by a source having a flux of ionizing photons equal to the flux of all the young hot stars. The same conclusion applies also to the other H series. Therefore Eqs. (3) and (7) have been adopted.

b) on the contrary the same simplification is not possible for the metallic lines and for such lines the integrated emission of the galaxy must be computed as the sum of the contributions of all the HII regions present, as consequence of Eq. (10). To this purpose we can imagine the galaxy as a complex of several HII regions each powered by a cluster of stars. This model is realistic since we observe that the majority of massive stars are born in groups. Depending on the SFR, and therefore on the number of young clusters, two situations can occur: a) the HII regions do not overlap each other: in this case the nebular emission of the galaxy is the sum of the contributions of all the HII regions; b) the HII regions partly or totally overlap: here the situation is more complex, but the extreme case can be adopted in which all the hot young stars of the galaxy power a unique large HII region. With a SFR equal to that actually measured in the disc of our galaxy and assuming a cluster mass of 3000 $M_\odot$ the sum of the volumes of all the HII regions is by several orders of magnitude smaller than the disc volume: the assumption that there is no overlap seems therefore a correct approximation for normal galaxies. Very likely only for mergers with a larger SFR a more correct model would be that of a single large HII region powered by all the young stars. The relations giving the luminosity of the H lines are still valid even in the case of overlap of the HII regions, since they imply only the total UV flux.

For each cluster of age τ the integrated luminosity $\mathscr{L}_{X_\lambda}(\tau)$ of the X_λ line has been obtained by approximating the integrated stellar spectrum with the spectrum of a single star with temperature T_{eq} and luminosity equal to the luminosity of the cluster. The equivalent star temperature has been determined by fitting the portion of the integrated spectrum of the cluster in the range 300–1000 Å to the corresponding portion of the stellar spectrum. The lower limit of such interval has been arbitrarily fixed at 300 Å. For smaller wavelengths the integrated spectrum is dominated by stars hotter than 50000 K, which is the upper limit of the temperatures of Kurucz's models. These stars are treated as black bodies, but this approximation is unsatisfactory and when the fitting is extended to $\lambda \leq 300$ Å too large equivalent temperatures ensue. It has been shown in fact with the hottest Kurucz' models that the monochromatic flux derived by the Plank law, for $\lambda < 300$ Å, is larger than that of the corresponding model.

The number of equivalent stars (i.e. those giving on the whole the same luminosity of the cluster) is equal to the ratio of photons emitted by the cluster stars to the photons emitted by

a main sequence (MS) star with $T_{eff} = T_{eq}$. The calibration of Panagia (1973) has been used for this purpose. One then gets:

$$\mathscr{L}_{X_\lambda}(\tau) = h_{X_\lambda}\mathscr{L}_{H\beta}(\tau) \tag{11}$$

where h_{X_λ} is derived from Stasinska's tables for the temperature of the equivalent star and interpolating in luminosity.

The integrated luminosity of the X_λ metallic line, as sum of the contributions of all the HII regions, is given by:

$$L_{X_\lambda} = \int_0^{\tau_M} \frac{dn_{cl}}{dt}\mathscr{L}_{X_\lambda}(\tau)d\tau \tag{12}$$

where dn_{cl}/dt is the number of clusters of given mass and age τ born in unit time.

2.3. The ionized gas emission: the continuum spectrum

The ionized gas has also a continuum emission chiefly arising from H and He. Let us at first consider the case of a single star. The continuous monochromatic luminosity per unit wavelength interval is obtained by:

$$L_c(\lambda) = \int_V N(H^+)N_e\gamma_T^c(\lambda)dV = N(H^+)N_e\gamma_T^c(\lambda)V \tag{13}$$

where $\gamma_T^c(\lambda)$ (Aller, 1984) includes the ratio χ of the radii of the ionization zones of He and H, accounting for the fact that the region where He is completely ionized once (the temperature of all the MS stars and WR stars is not so high to ionize He twice) does not necessarily coincide with the region where H is completely ionized. The behaviour of χ with the temperature of the exciting star is given by Osterbrock (1989).

$L_c(\lambda)$ depends on the volume of the ionized region, which can be eliminated with the relation:

$$n_c = N(H^+)N_e\alpha_B V \tag{14}$$

where the homogeneity of the HII region has been assumed; n_c is the UV flux. Relation (14) is derived from the ionization balance. One then gets:

$$L_c(\lambda) = \frac{\gamma_T^c}{\alpha_B}n_c \tag{15}$$

Since we have approximated the integrated spectrum of each cluster with the spectrum of an equivalent star, the continuous monochromatic luminosity of the region powered by a cluster is given by:

$$\mathscr{L}_c(\lambda,\tau) = \frac{\gamma_T^c(\lambda)}{\alpha_B}.\mathscr{N}_c^*(\tau) \tag{16}$$

where $\mathscr{N}_c^*$ is the ionizing flux of the equivalent star; the factor χ is function of the temperature of the equivalent star and is evaluated from Fig. 2.5 of Osterbrock (1989). Table 1 shows the calibration as function of the age for a star cluster with solar composition and an initial mass M_{cl} = 3000 $M_\odot$.

Table 1. Adopted calibration values for a star cluster of different ages: temperature of the equivalent star, adopted χ parameter and logarithm of the number of ionizing photons

Age ($10^6 yr$)	$T_{equiv.}$ (kelvin)	χ	log NUV (M_{cl} = 3000$M_\odot$)
1	45000	1	49.213
3	45000	1	49.301
4	40000	1	48.935
10	40000	1	47.876
40	19000	0	43.739

The continuous monochromatic luminosity of the galaxy is derived by summing up the contributions of all the HII regions:

$$L_c(\lambda) = \int_0^{\tau_M} \frac{dn_{cl}}{dt}L_c(\lambda,\tau)d\tau \tag{17}$$

dn_{cl}/dt being the number of star clusters born per unit time at t.

The results obtained by approximating the integrated spectrum of the cluster with the spectrum of a star with suitable temperature have been compared with models derived with the photoionization program Cloudy (Ferland, 1991) in which the integrated spectrum of the cluster has been used: the differences are below the uncertainties connected with the assumptions and with the precision with which the input physics is computed. The program Cloudy has been also used to supplement the calibration at low temperatures (T_e = 19000 K).

The results depend obviously on the parameters taken to characterize the clusters: a) the IMF and the upper limit of the stellar masses; throughout this paper a Salpeter IMF with x=-1.35 and masses in the range 0.01-100 $M_\odot$ have been adopted; b) the total number of ionizing stars in the cluster (this parameter can be changed in order to treat normal open clusters or more massive groups like globular or globular-like clusters); c) the chemical composition and the density of the gas. Generally the solar composition has been adopted with a temperature of 8000 K for the ionized gas while its density is taken to be n = 10 cm^{-3}. A simple calculation of the dynamical evolution of an HII region shows that the electron density evolves from the initial value corresponding to the original density of the molecular gas (n=$10^3 cm^{-3}$) by two orders of magnitudes. Moreover from the ratio of the SII lines in HII regions in spiral galaxies Zaritsky et al. (1994) find densities "smaller than about 100 cm^{-3}". Converting Zaritsky et al. line ratios to densities according to Czyzak et al. (1986), densities typically less than 50 cm^{-3} are found.

3. Models and comparison with Kennicutt's spectra

The two components of the spectrum, the stellar and gaseous components, are correlated in the sense that the ionizing flux must be computed with the same number of young hot stars which enter in the computation of the stellar spectrum. To this

Table 2. Model results as a function of the spectral type. A positive value of the EW($H\delta$) indicates the line is in absorption, while the opposite is true for the other lines. Results for the three Balmer lines are shown for emission only (emis) and including both absorption and emission (tot). Also shown are the "Extreme" model (constantly increasing SFR) and the metal poor elliptical model (Emp) with average Z=0.001

Type	D_{4000}	EW(OII)	EW($H\delta$) (tot)	EW($H\alpha$) (tot)	EW($H\beta$) (tot)	EW(OIII)	EW($H\delta$) (emis)	EW($H\alpha$) (emis)	EW($H\beta$) (emis)
E	2.21	0.0	0.9	-1.0	-1.7	0.0	–	–	–
Sa	1.91	4.7	1.1	1.7	-2.2	2.0	-0.4	3.2	1.2
Sb	1.75	9.0	1.0	6.0	-0.7	4.7	-0.9	7.8	2.8
Sc	1.54	14.9	1.4	16.5	1.7	10.2	-1.8	19.2	6.3
Sd	1.42	17.3	1.7	26.3	3.4	14.1	-2.4	29.6	9.0
Ex	1.31	21.7	1.2	47.4	6.8	21.9	-3.3	52.8	14.6
Emp	1.72	0.0	1.2	-1.0	-1.7	0.0	–	–	–

Table 3. Model results as a function of the spectral type: colour indices

Type	(1550-V)	(U-B)	(B-V)	(V-R)	(R-I)	(g-r)	(r-i)	(U-685)	(B_j - R_f)
E	5.37	0.50	0.93	0.74	0.65	0.71	0.39	2.77	1.71
Sa	1.09	0.31	0.83	0.68	0.57	0.64	0.33	2.40	1.56
Sb	0.16	0.19	0.76	0.65	0.56	0.60	0.32	2.19	1.47
Sc	-0.74	0.00	0.63	0.58	0.52	0.52	0.29	1.80	1.29
Sd	-1.17	-0.11	0.53	0.52	0.46	0.44	0.25	1.52	1.14
Ex	-1.72	-0.24	0.39	0.45	0.44	0.34	0.23	1.18	0.94
Emp	3.79	0.21	0.77	0.58	0.44	0.55	0.23	2.15	1.43

aim the absolute visual magnitude of the galaxy has been a priori fixed; this corresponds to determine the value of the product of the normalization constant in the IMF and of the value of the initial SFR ψ_o.

Besides the first eight lines of the Balmer series and the L_α line at 1215 Å, the following lines have been synthesized: HeI5876, CII2326, CIII1909, CIV1549, NII5755, NII6584, OI6300, OII3727, OII7325, OIII4363, OIII5007, NeIII3869, MgII2798, SII4070, SII6720, SII6312.

To determine the equivalent widths the ratio of the line flux to the total (stars + gas) flux at the central wavelength λ_0 of the line is computed. The fluxes of the H lines, given by Eq. (7), are distributed over a gaussian profile:

$$I = \frac{I_0}{\sqrt{2\pi}\sigma} exp \frac{-(\lambda - \lambda_0)^2}{2\sigma^2} \quad (18)$$

σ is such that the width of the absorption line is larger than that of the emission component. The equivalent width is then computed with a semi-automatic procedure using the program SPLOT in IRAF.

Models have been derived to describe galaxies of several morphological types (elliptical, Sa, Sb, Sc, Sd); the model labelled "Extreme" has a SFR monotonically increasing along all its evolution and its metallicity evolves approximately as in the Sd model. A further model has been derived with a SFR typical of an elliptical, however with a smaller average metal content (Emp, Z=0.001): this model allows to study the influence on colour indices and spectral features of the metallicity and corresponds to a very extreme case since ellipticals with such a low metal content should be very faint.

The SFR adopted for normal galaxies of the morphological sequence have been derived with a simple model of chemical evolution constrained with the broad band UBVRI colours, the present average metal abundance and the fraction of gaseous mass to the total mass. The SFRs thus obtained are very similar to those derived by Sandage (1986) and are given in the Appendix. An age of 15 Gyr has been adopted.

The spectrum of the nebular component has been computed according to the prescriptions of Sect. 3 with clusters of solar metallicity and an initial mass of 3000 $M_\odot$.

Some spectral features and colours of such models are presented in Table 2 and Table 3. The uncertainty affecting the equivalent width of the $H\beta$ line is larger than for other lines, due the difficulty of estimating the level of the continuum. Corresponding to maximum and mimimum estimate of it, two extreme value have been obtained for each model and their average is shown in Table 2. The inspection of the tables allows the estimate of the relative importance of the two components (stellar in absorption and nebular in emission) of the $H\alpha$, $H\beta$ and $H\delta$ lines. The models also show that the colours of normal spirals are not significantly affected nor by the nebular continuum nor by the emission lines. In fact the contribution of the gaseous continuous emission in spiral models is by more than two orders of magnitude smaller than the stellar contribution. Only in the case of very strong bursts both components are comparable.

A comparison with HII region models (Olofsson 1989, Garcia-Vargas et al. 1995, Mayya 1995, Stasinska & Leitherer 1996 and references therein) is not straightforward, since in this work we *make use* of HII region models (Stasinska 1990) in order to study the integrated spectrum of galaxies.

In the following analysis we compare our results with observed galaxy spectra, considering a subsample of Kennicutt (1992a) atlas consisting of 33 high resolution (5 - 8 Å) spectra and 6 medium resolution (15 - 25 Å) spectra covering the 3500-7500 Å interval. This sample includes galaxies of all the

Table 4. Normal galaxies in Kennicutt's sample: (1) name; (2) morphological type; (3) an asterisk indicates a low resolution spectrum; (4) D_{4000}; (5),(6),(7),(8),(9) equivalent widths in Å; note that a positive value of the EW($H\delta$) indicates the line is in absorption, while the opposite is true for the other lines; (10),(11) fully corrected colours from the Third Reference Catalogue of Bright Galaxies (De Vaucoulers et al. 1991)

Name	Type	Res	D_{4000}	EW(OII)	EW($H\delta$)	EW($H\alpha$)	EW($H\beta$)	EW(OIII)	$(B-V)$	$(U-B)$
(1)	(2)	(3)	(4)	(5)	(6)	(7)	(8)	(9)	(10)	(11)
NGC3379	E0		2.23	0.0	0.7	–	-2.0	0.0	0.94	0.52
NGC4472	E1/S0	*	2.10	0.0	0.0	-1.0	-1.4	0.0	0.95	0.56
NGC4648	E3		2.22	0.0	0.9	-1.0	-2.0	0.0	0.89	0.51
NGC4889	E4		2.26	0.0	0.0	–	–	0.0	0.97	0.54
NGC3245	S0		2.09	0.0	0.7	-0.9	-2.5	0.0	0.86	0.44
NGC5866	S0	*	2.00	0.0	0.0	–	–	0.0	0.79	0.33
NGC4262	SB0		2.13	2.0	1.2	–	–	–	0.90	0.49
NGC3941	SB0/a		2.17	1.0	1.1	–	–	–	0.88	0.43
NGC1357	Sa		1.84	4.0	1.7	5.4	-2.5	< 0.3	0.80	0.20
NGC2775	Sa		2.00	1.6	1.2	1.1	-4.0	< 0.5	0.85	0.33
NGC3623	Sa		2.10	1.5	1.4	0.7	-3.0	< 0.5	0.81	0.35
NGC3368	Sab		1.97	4.0	1.5	1.7	-3.5	< 0.5	0.81	0.27
NGC3147	Sb		1.79	3.0	1.9	7.5	-1.0	< 0.5	0.78	–
NGC3627	Sb		1.60	5.0	3.1	13.7	-3.0	< 0.4	0.66	0.14
NGC1832	SBb		1.50	17.0	1.8	23.8	0.0	2.0	0.54	-0.08
NGC5248	Sbc		1.52	9.0	2.3	21.8	1.0	1.0	0.62	0.02
NGC6217	SBbc		1.55	12.0	3.2	26.1	0.0	2.0	0.57	-0.22
NGC2903	Sc		1.54	8.0	3.1	19.0	-1.5	< 0.6	0.59	0.00
NGC4631	Sc		1.32	40.0	3.6	49.6	4.0	15.0	0.41	–
NGC6181	Sc		1.43	15.0	2.3	33.3	1.5	3.5	0.49	-0.13
NGC6643	Sc		1.60	11.0	3.7	25.4	0.0	1.5	0.52	-0.13
NGC4775	Sc		1.29	35.0	2.1	45.9	6.0	14.0	–	–

Table 5. As Table 4 for irregulars and peculiar galaxies. Symbols in the last column (from Kennicutt): (a) spectrum with high Galactic reddening; (b) interacting/merging; (c) starburst nucleus; (d) E+A; (e) global starburst; (f) aperture centered on the dominant HII region in large galaxy

Name	Type	Res	D_{4000}	EW(OII)	EW($H\delta$)	EW($H\alpha$)	EW($H\beta$)	EW(OIII)	$(B-V)$	$(U-B)$	Notes
(1)	(2)	(3)	(4)	(5)	(6)	(7)	(8)	(9)	(10)	(11)	(12)
NGC4449	Sm/Im		1.27	55.0	1.9	75.0	11.0	33.0	0.37	-0.38	
NGC1569	Sm/Im		1.40	49.0	0.4	121.7	35.0	182.0	–	–	(a)
Mrk59	SBm/Im	*	0.79	62.0	-8.2	765.0	115.0	750.0	–	–	(f)
Mrk71	SBm	*	0.82	108.0	-60.0	1323.5	299.0	2490.0	–	–	(f)
NGC4485	Sm/Im		1.30	48.0	2.2	59.1	4.0	33.0	0.35	-0.25	(b)
NGC2276	Scpec		1.25	33.0	1.0	64.6	7.0	10.0	0.45	-0.14	(b)
NGC3690	Scpec	*	1.14	48.0	0.0	168.3	22.0	30.0	0.59	0.04	(b)
NGC3303	Pec	*	1.89	35.0	3.2	–	-3.0	2.0	–	–	(b)
NGC7714	Spec		1.03	59.0	-1.7	139.8	22.0	41.0	0.44	-0.51	(b) (c)
NGC2798	Sapec		1.53	17.0	2.1	41.7	1.0	3.0	0.63	-0.07	(b) (c)
NGC3921	S0pec		1.78	11.0	4.5	8.5	-3.0	< 0.5	0.59	0.26	(b) (d)
NGC3310	Sbcpec		1.19	63.0	0.3	126.4	20.0	48.0	0.32	-0.45	(e)
UGC6697	Spec		1.16	44.0	1.1	62.6	8.0	22.0	0.28	-0.48	
NGC4750	Sbpec		1.66	5.0	2.0	10.4	-2.0	< 0.5	–	–	
NGC4670	SBpec		1.32	62.0	2.1	93.4	22.0	54.0	0.36	-0.50	

Table 6. Ratio of the past average SFR to the present SFR $< \psi > / \psi(T)$ as a function of D_{4000}; the average past SFR is obtained over three time intervals: 1, 5 and 16 Gyr

β (Gyr^{-1})	D_{4000}	$< \psi > / \psi(T)$ δt = 1 Gyr	$< \psi > / \psi(T)$ δt = 5 Gyr	$< \psi > / \psi(T)$ δt = 15 Gyr
1.0	2.21	1.72	29.48	5.55×10^5
0.7	2.20	1.45	9.18	6.53×10^3
0.5	2.15	1.30	4.47	3.72×10^2
0.3	1.87	1.17	2.32	2.51×10^1
0.2	1.65	1.11	1.72	7.35
0.1	1.48	1.05	1.30	2.47
0.05	1.42	1.03	1.14	1.53
0.01	1.38	1.01	1.03	1.08

normal types. AGNs, in which the interstellar gas is, at least partly, ionized by a nonthermal component, are not considered.

A few samples of integrated spectra of nearby galaxies, including the contribution of all the galaxy, are available. There are in the literature many spectra of nuclear regions but they cannot be used to describe the behaviour of the whole galaxy, due to gradients of the metallicity of the gas and stellar populations. Moreover they cannot be compared with the spectra of distant galaxies, whose projected aperture diameter is typically of several kpc. The consequence of this undersampling is the underestimate of the emission lines, since in several galaxies the stellar continuum emission (originating from the disk and the bulge) is more centrally condensed than the disk nebular emission.

From the spectra of his sample Kennicutt (1992a, 1992b) has derived the following quantities: the morphological type, the absolute magnitude M(B), the equivalent width of the $H\alpha$ + [NII]$\lambda\lambda$6548-6583 blend, a continuum colour index "41-50", the [NII]/$H\alpha$ flux ratio, the equivalent widths and the flux ratios related to $H\alpha$ + [NII] of the following lines: [OII]λ3727, $H\beta$, [OIII]λ5007, [SII]$\lambda\lambda$6717,6731. Uncertainties affecting such data range from 5 to 10 % for the galaxies with the strongest emission lines to 30 % for galaxies with the faintest lines. We have implemented this panorama of data by computing from Kennicutt's spectra the quantity D_{4000} and the equivalent width of the $H\delta$ line for all the considered objects and the equivalent widths of the [OII] and $H\beta$ lines of E and S0 galaxies, when possible. Furthermore the equivalent width of the $H\alpha$ line has been derived from Kennicutt's $H\alpha$ + [NII] equivalent width and from [NII]/$H\alpha$ flux ratios.

The equivalent widths have been computed with the same method used for the synthetic spectra, the SPLOT program in IRAF. The level of the continuum and the wavelength interval have been chosen interactively each time and in the most difficult cases the measure has been repeated. When necessary the redshift has been determined through the identification of the OII line at λ= 3727 Å and of the $H\alpha$ line in the case of emission line galaxies; in early type galaxies the redshift value derived by Kennicutt has been adopted. The equivalent widths thus determined are affected by uncertainties similar to those given by Kennicutt: in the case of the $H\delta$ line the uncertainty is of the order of 15 %, for strong lines it tends to be smaller and can reach also 30 % if an emission component is present.

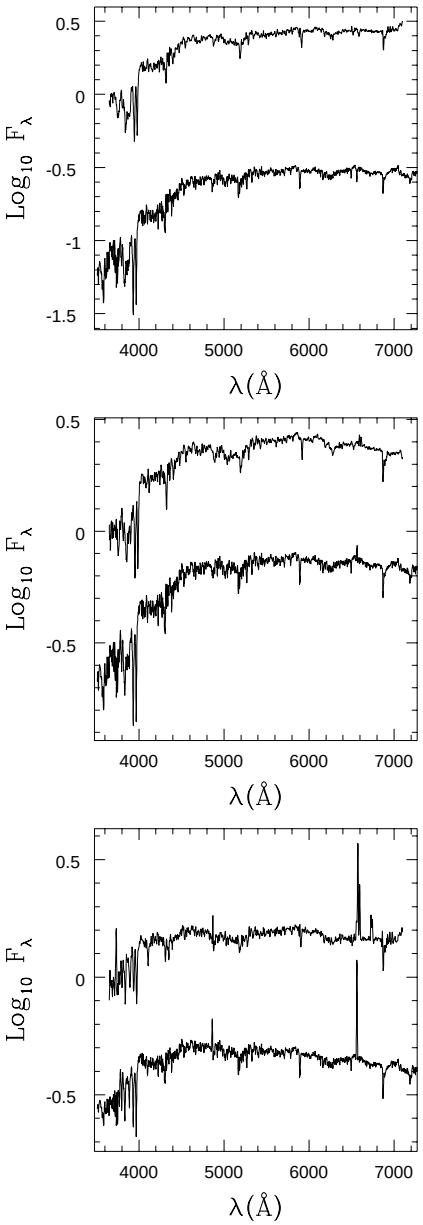

Fig. 1a–c. Comparison between observed and synthetic spectra, in arbitrary flux units: **a** NGC3379 (top) and elliptical model (bottom), **b** NGC2775 (top) and Sa model (bottom), **c** NGC2903 (top) and Sc model (bottom).

In Tables 4 and 5 all these quantities are collected for normal ellipticals and spirals and for irregular and peculiar galaxies respectively.

In Fig. 1a the spectrum of the galaxy NGC 3379 belonging to Kennicutt's sample is compared with the elliptical model. Both emission lines and strong Balmer absorption lines are absent. The Sa galaxy NGC 2775 together with the correspondig

model is shown in Fig. 1b: the $H\alpha$ line in emission, although faint, is present, while D_{4000} is decreased in comparison to the elliptical: anyway this feature can be hardly appreciated by a simple eye inspection of the spectrum. The changes are more evident when a Sc galaxy is considered as is the case of Fig. 1c where NGC 2903 is presented with its model: the $H\alpha$ and $H\beta$ in emission are evident. In the observed spectrum also the [OII]λ3727 is present while in the model the metallic lines are not shown although they are computed and their equivalent widhts are presented in Table 2.

4. Spectroscopic features affected by young stars

In this section we analyze the behaviour of the spectral features which are directly or indirectly connected with the presence of young stars as the Balmer lines in emission or the [OII] line at λ = 3727 Å. The maximum and the average values of the equivalent width of the [OII] line increases towards late galactic types and the spread within each morphological type is considerably large, as shown by Kennicutt (1992b). The trend with the type is also confirmed by the models. Peculiar galaxies (mergers and starbursts) cover a wide range of values but they have predominantly the largest equivalent widths ($EW > 40$ Å), not reached by normal galaxies.

The correlation between equivalent widths of [OII] and $H\beta$ lines is presented in Fig. 2: within the errors there is agreement between the theoretical results and the observations. Galaxies Mk 59 and Mk 71 are not reproduced in the figure: these objects, which share the features of HII regions, deviate from the relation and have a high EW($H\beta$)/EW([OII]) ratio (> 1.8) compared with the typical values (< 1) found for spirals and irregulars.

A further test is provided by the sample of 21 nearby blue cluster or field galaxies, mainly Sb and Sc collected by Dressler and Gunn (1982). Also in this case spectra cover the whole galaxy ($\simeq$ 15 kpc). Again the observed $H\beta$ - [OII] relation is reproduced with good accuracy by the models.

This strong correlation is confirmed, for normal spiral galaxies, by the models of Stasinska & Leitherer (1996): they found that, if the number of ionizing stars of an HII region is relatively small ($\approx$ 50), the $H\beta$/[OII] ratio is only marginally dependent on age (it is increasing with the age of the starburst, levelling off after a certain time), while it does depend on the electron density. Since the equivalent width of the $H\beta$ emission line correlates with the SFR, also EW([OII]) is a good SFR indicator. However Stasinska & Leitherer (1996) found that this behaviour fails when the number of ionizing stars is considerably increased. Therefore the SFR–[OII] calibration is applicable to late–type galaxies, where the mass range of star clusters and the electron density range (Zaritsky et al. 1994) are apparently limited. On the contrary, even in conditions typical of spiral galaxies the $H\beta$/[OIII] ratio is strongly affected by the excitation parameters.

For a given [OII] equivalent width, models tend to have EW($H\alpha$) smaller than observed, anyway differences are comparable to the uncertainty in the evaluation of the equivalent width, considering the variation of the ratio $H\alpha$/[OII] with the metallicity and the difficulty in measuring the $H\alpha$ line due to the NII blend in the observed spectra.

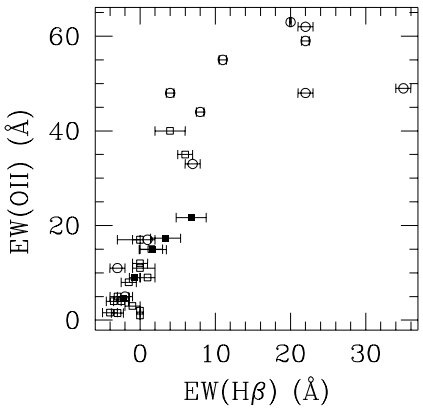

Fig. 2. Equivalent widths of [OII] and $H\beta$ of the galaxies of Kennicutt's sample (empty symbols: squares are ellipticals and spirals from Table 4, circles are irregular and peculiar galaxies from Table 5) and models (filled symbols). The error bars indicate the uncertainties in the placement of the continuum

Other emission lines have been computed. In Fig. 3a and Fig. 3b the observed relations of [SII]6716,6731 with H_α and (U-B) are shown and both are nicely reproduced by the models. The [OIII] line is instead clearly overestimated in the models. In this case the disagreement cannot be attributed to the procedure of measuring the equivalent width from the spectra. This line drastically depends on the excitation conditions within the HII regions, known to present large variations within each galaxy. This is the reason why the [OIII] line is not fit for determining the SFR. The fact that models systematically yield too large [OIII] values seems to suggest that the effective temperatures adopted for the stars responsible for the ionization of the interstellar gas may have been overestimated. This can be consequence both of the way in which the equivalent stars are determined for the clusters powering the HII regions and the inadequacy of Kurucz models for very hot stars for $\lambda < 1000$ Å. Another possibility is the need of adopting a different metal content in computing the gaseous emission. In fact the measured abundance properties in nearby spiral galaxies (Zaritsky et al. 1994) seem to indicate an oxygen content higher than solar. An inspection of Stasinska's tables shows that when the solar metallicity is increased by a factor 2, the ratio OIII/Hβ decreases by a factor 8.

Another source of uncertainty are the parameters of the IMF. While the slope of the IMF seems not crucial in determining the stellar spectrum in young stellar populations (Barbaro & Olivi 1991), a larger influence arises from the upper mass limit. Decreasing such a limit the average temperature of the stars responsible for the excitation of the HII region is lowered and again the ratio OIII/Hβ is significantly reduced, as it can be derived from Stasinska's models. Unfortunately there is no firm evidence of the most appropriate values of such a parameter and its dependence on the environmental conditions.

Another quantity affecting the line ratios is the electron density but an inspection of Stasinska's models shows that in order

Table 7. SFRs of the galaxies in Kennicutt's sample. Values of β in Gyr^{-1} are derived from the observed (U-B) by using Fig. 6. The luminosities L_V and L_U are derived from the models and are given in the tables in units $10^{42} ergs\, s^{-1}$. Present SFRs are obtained with two methods (see text for details)

name	type	(U-B)	beta	M_B	L_V	L_U	EW(OII)	ψ_0	SFR^1	SFR^2	b
(1)	(2)	(3)	(4)	(5)	(6)	(7)	(8)	(9)	(10)	(11)	(12)
n3379	E0	0.52	1.00	-19.7	7.12	1.32	0	53	6×10^{-5}	–	1.8×10^{-6}
n4472	E1/S0	0.56	1.00	-21.5	37.38	6.94	0	–	–	–	1.8×10^{-6}
n4648	E3	0.51	1.00	-19.0	3.74	6.94	0	30	3×10^{-5}	–	1.8×10^{-6}
n4889	E4	0.54	1.00	-22.1	64.96	12.06	0	–	–	–	1.8×10^{-6}
n3245	S0	0.44	0.44	-19.3	4.83	0.96	0	37	0.14	–	0.0062
n5866	S0	0.33	0.30	-19.3	4.54	1.09	0	27	0.7	–	0.0398
n4262	SB0	0.49	0.55	-18.4	2.13	0.41	2	16	0.013	0.15	0.0013
n3941	SB0/a	0.43	0.43	-19.2	4.39	0.88	1	33	0.15	0.23	0.0071
n1357	Sa	0.20	0.23	-20.2	9.78	2.81	4	57	3.3	1.7	0.0952
n2775	Sa	0.33	0.30	-19.9	7.90	1.89	1.6	50	1.2	0.63	0.0398
n3623	Sa	0.35	0.33	-20.6	15.36	3.47	1.5	110	1.8	1.1	0.0270
n3368	Sab	0.27	0.27	-20.5	13.42	3.45	4	87	3.1	2.0	0.0582
n3147	Sb	–	-	-22.0	–	3.00	–	–	–	–	
n3627	Sb	0.14	0.20	-19.9	7.18	2.26	5	38	3.1	1.6	0.1360
n1832	SBb	-0.08	0.10	-20.6	12.09	5.17	17	63	12.7	10.3	0.4047
n5248	Sbc	0.02	0.11	-20.3	9.29	3.86	9	45	8.5	4.4	0.3657
n6217	SBbc	-0.22	< 0.001	-20.2	7.51	4.07	12	–	–	6.0	0.9992
n2903	Sc	0.00	0.11	-20.1	7.73	3.21	8	28	5.3	3.3	0.3657
n4631	Sc	–	–	-20.5	–	40	–	–	–	–	
n6181	Sc	-0.13	0.03	-20.7	12.26	6.25	15	75	13.9	11.1	0.7791
n6643	Sc	-0.13	0.03	-20.7	12.26	6.25	11	75	13.9	8.4	0.7791
n4775	Sc	–	–	-19.9	–	35	–	–	–	–	

to reduce the OIII/Hβ ratio smaller unrealistic values of the density are required.

5. Spectroscopic features affected by relatively old stars

The spectral features till now considered are related to the presence of stars born in the last few ten million years. In the following we consider other quantities which are the signature of stars born in previous times.

The break at 4000 Å D_{4000} has been often used as age indicator of distant galaxies neglecting its dependence on the metallicity. In Fig. 4 D_{4000} is plotted against the equivalent width of the H_α line both for normal galaxies and peculiar ones. The normal galaxies define a tight relation while peculiar objects exhibit a large spread. This behaviour is expected since H_α is affected only by the very young stars while D_{4000} is influenced also by older stars. A consequence of these consideration is that the most intense bursts in peculiar galaxies of Kennicutt's sample must involve a large number of young stars. They in fact have very small values of D_{4000}, not reached by any normal galaxy however late it is. Nevertheless D_{4000}, as other spectral features, is able to discriminate between normal and peculiar galaxies only in the most extreme cases.

The D_{4000} - OII and D_{4000} - H_β relations are very similar and lead to the same conclusions: D_{4000} is a good age indicator only in the case of normal galaxies, but fails in the case of starbursts.

Unlike the Balmer lines up to now considered, the $H\delta$ line is always observed in absorption in the spectra of spiral galaxies, since the stellar absorption overwhelmes the gaseous emission. Most of the normal galaxies of the sample have EW($H\delta$) $<$ 3.2 Å. Only two Sc spirals have 3.2 $<$ EW($H\delta$) $<$ 4. All the peculiar objects, with the exception of the "E+A" galaxy, have EW($H\delta$) < 2 and in the spectra of many of them the line is emission-filled. Based on our models, emission $H\delta$ lines are expected only in the spectra of objects with a current intense starburst.

Strong absorption $H\delta$ lines instead are typical of galaxies which have experienced in the past an intense burst of star formation ended about 1 - 2 gyr ago. Their spectra can be interpreted as the superposition of a normal galaxy (elliptical or spiral) and a generation of A stars (Dressler & Gunn 1982). A detailed analysis (Poggianti and Barbaro, 1996) dealing with all stars having enhanced $H\delta$ absorption confirms the validity of this interpretation. In the adopted sample this is the case of NGC 3921, which due to the strong absorption Balmer line has been classified as E+A. This interacting galaxy is probably in an advanced burst phase or even in a post-burst phase in which the emission lines are weak and the absorption feature begin to emerge.

The equivalent widths of the $H\alpha$ and [OII] lines are well correlated with (U-B) e (B-V) colours (Fig. 5a and Fig. 5b) and

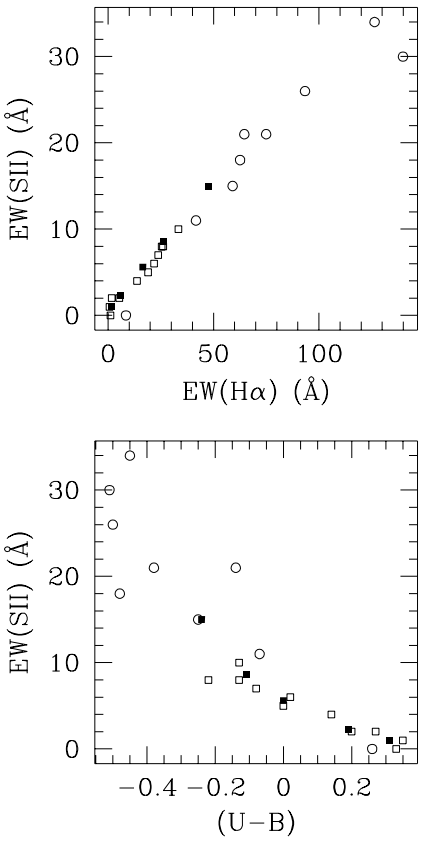

Fig. 3a and b. [SII] equivalent widths versus EW($H\alpha$) (**a**) and (U-B) colour index (**b**) ; symbols as in Fig. 2

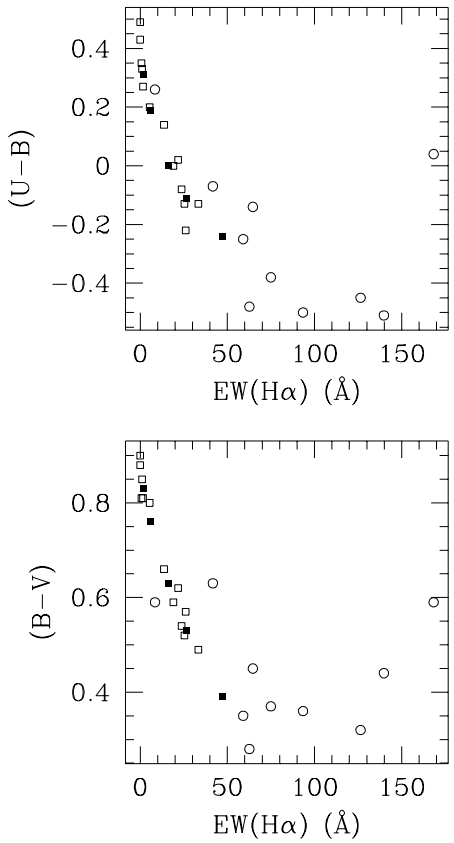

Fig. 5a and b. Comparison emission line–colours; symbols as in Fig. 2

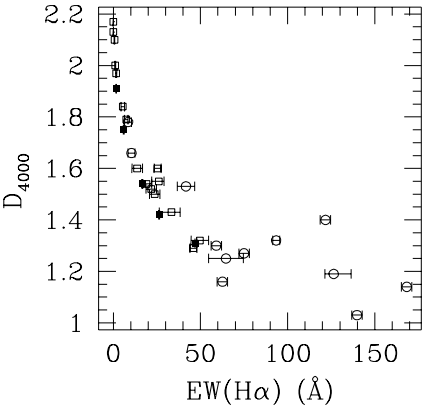

Fig. 4. D_{4000} versus EW($H\alpha$); symbols as in Fig. 2

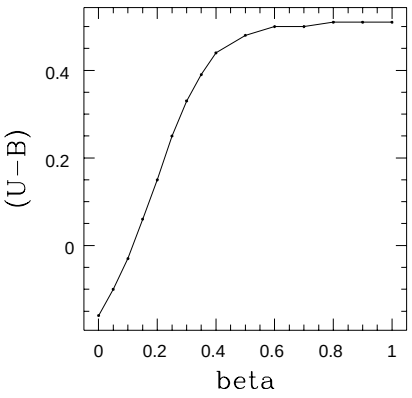

Fig. 6. (U-B) color index versus β (Gyr^{-1}) for models with an analytical SFR (Eq. 19)

these relations are nicely fitted by the models of normal galaxies (in such diagrams E-Sa-Sb-Sc-Sd models are shown). The correlations between the colours and the equivalent widths become weaker in the case of peculiar galaxies; these objects show an excess of emission with respect to what is expected by extrapolating the relation found for normal galaxies. The information emerging from the (U-B) e (B-V) colours is therefore equivalent to that supplied from the spectral features in the case of a galaxy whose star formation history did not show sudden changes.

We have seen that a net flux of the $H\delta$ line in emission testifies the presence of a current burst while a strong absorption feature is indicative of a burst ended some 1 - 2 Gyr ago. Some starbursts can be also identified by their extremely blue colours or very low D_{4000} values (see Tables 2 and 3 for the lowest values of colours and D_{4000} for normal galaxies, given by the "Extreme" case).

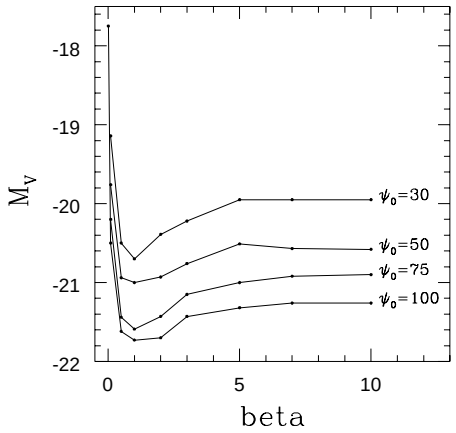

Fig. 7. M_V magnitude as a function of β for different values of ψ_0

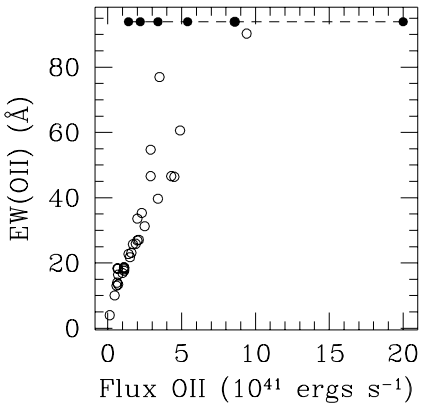

Fig. 8. Fluxes and equivalent widths of [OII] for a series of burst models in ellipticals and spirals with $M_B = -20$ (open circles) with different burst parameters; the dashed line connects models with the same SF history and different absolute magnitudes (filled circles, from left to right $M_B = -18, -18.5, -19, -19.5, -20, -21$)

6. Evaluation of the star formation rate

In this section an attempt is made to exploit the general features of the models and the peculiar characteristics of some quantities to derive estimates of the star formation rates in normal and starburst galaxies. A first evaluation, limited to the normal galaxies of the Hubble sequence, can be obtained from purely photometric data. To this aim spectrophotometric models have been derived by using an analytical SFR of the type:

$$\psi(t) = \psi_o \beta exp(-\beta t) \tag{19}$$

This relation is a fairly good approximation of the SFR so far adopted and represents a suitable parametrization. The β parameter is related to the timescale of the star formation, ψ_o depends on the galaxy mass. The UBV colours depend solely on the relative distribution of stars of different age and therefore are function of β alone. With a SFR of this type and with convenient values of β the colours of the different morphological types are satisfactory reproduced.

The (U-B) colour index as a function of β is shown in Fig. 6. Provided that the correction for reddening is determined it is an easy matter to derive with this relation the value of β. To ignore the reddening correction implies an overestimate of the β value.

The luminosities in the different photometric bands are instead function both of β and of the galaxy mass and therefore of ψ_o. In Fig. 7 the M_V magnitude is plotted against β for several values of ψ_o: entering this diagram with M_V and β, the value of ψ_o can be determined and consequently both parameters of $\psi(t)$ are estimated.

A further calibration can be derived for late-type galaxies in terms of the D_{4000} index. We still use the expression (19) for $\psi(t)$. For each value of β the ratio $< \psi > /\psi(T)$ between the average value of ψ over the time interval (T- δt,T) and the present value of ψ can be derived. The average value is given by:

$$< \psi >= \frac{1}{\delta t} \int_{T-\delta t}^{T} \psi_o \beta exp(-\beta t) dt \tag{20}$$

$$= \frac{\psi_o \beta}{\delta t} \frac{exp(-\beta(T-\delta t) - exp(-\beta T)}{\beta} \tag{21}$$

One then gets:

$$\frac{< \psi >}{\psi(T)} = \frac{exp(\beta \delta t) - 1}{\beta \delta t} \tag{22}$$

This quantity can be easily computed as a function of β for several values of δt: only for large values of δt does the function $< \psi > /\psi(T)$ vary over a sufficient large interval allowing an accurate evaluation. Therefore we adopt δt = 1, 5 and 16 Gyr. From (22) and from the D_{4000} - β relation derived from the models the calibration $< \psi > /\psi(T) - D_{4000}$, shown in Table 6, is obtained. From the observed value of D_{4000} the ratio $< \psi > /\psi(T)$ is then estimated and, if $\psi(T)$ is derived from one method described in the following, the average SFR over the last billion years can be evaluated. Since $\psi(T)$ can be determined only for late-type galaxies the method is restricted to object with $D_{4000} < 2.1$. The same calibration is obtained using a non analytical SFR, as in the majority of the models considered in this work. Note that $< \psi > /\psi(T)$ for δt = 16 Gyr is the inverse of the Scalo's (1986) b parameter.

In particular Eq. (19) allows the determination of the present SFR. This quantity can be estimated also from the spectral features, in particular from the emission nebular lines. In ionization-bound HII regions the luminosity of the Balmer emission lines is, to a first approximation, independent of the temperature of the gas and is only related to the total ionizing flux of hot young stars (Osterbrock 1989). This is the theoretical reason for deriving the formation rate of massive stars from the Balmer line fluxes. When an estimate of the IMF is made, the total SFR can be also derived. A series of models of spirals of different morphological types with $M_B = -18$ mag and $M_B = -20$ mag has been computed in order to derive the relations between the SFR (in $M_\odot\, yr^{-1}$) and the luminosities of the $H\alpha$ and OII lines (in $ergs\, s^{-1}$) and their equivalent widths.

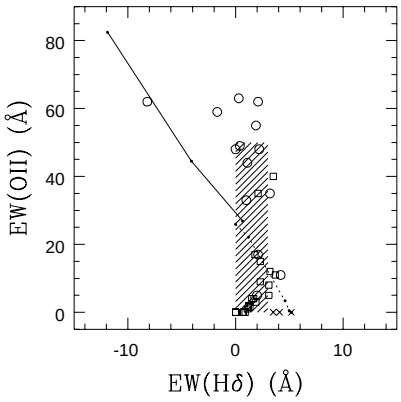

Fig. 9. EW(OII) versus EW($H\delta$). The shaded area represents the region of the diagram where models of the normal spectral types lie. In such area, the highest EWs(OII) can be reached considering less than solar metallicities. Burst models with different burst lenghts and constant intensity are connected by the solid line: from left to right the points indicate bursts with lenght 10, 100 and 1000 Myr. Post-starburst models in which the star formation is truncated at the end of the burst are also shown: crosses represent models of a burst in a Sc spiral galaxy in which the star formation ended 100 Myr ago and involving 0.3, 3 and 26 % of the galactic mass (from left to right). The dashed line shows the time evolution of the 26 % model at 0,1,10,30,100 Myr after the end of the burst (from left to right). Kennicutt's data are presented as open symbols (squares are ellipticals and spirals, circles are irregulars and peculiar galaxies). See text for details

Using spiral models later than Sa one has for the luminosity of the $H\alpha$ line:

$$\psi = 4 \times 10^{-41} L(H\alpha) \quad (23)$$

This calibration can be compared with a similar relation found by Kennicutt (1983) in which the numerical coefficient is 2.3×10^{-41}. The difference is partly due to different IMFs used in the two calibrations. Kennicutt (1983) argues that the Hα line is the best feature for estimating the SFR and he points out that for distant galaxies, due to redshift, the Hα line falls outside the visible spectrum and in its place the [OII] line is usually employed. From the set of our models the following relation has been derived:

$$\psi = 6.3 \times 10^{-41} L(OII) \quad (24)$$

Since the [OII] line flux is related to the total number of massive stars able to ionize the gas and since the maximum main sequence lifetime of these stars is some ten million years, ψ is the SFR averaged over the last 10^7 yr. This relation is universal in the sense that it does not depend on the overall history of the star formation and therefore it applies both to normal galaxies and to starbursts and, provided that there has been no abrupt change, can be thought as the present SFR. Of course if the burst started less than 10^7 yr the SFR cannot be derived from the [OII] flux unless the length of the burst can be guessed.

Starting from his calibration equivalent to (23) and using a relation between the Hα and [OII] fluxes, derived from his sample, Kennicutt (1992b) obtained an analogous relation for the luminosity of the [OII] line :

$$\psi(M_\odot yr^{-1}) = 5.0 \times 10^{-41} L([OII]) \quad (25)$$

to be compared with our Eq. (24). The differences between (24) and (25) are of the same order of magnitude as in the L($H\alpha$) – ψ relations. The uncertainty affecting Eq. (25) are more important than that of L($H\alpha$) – ψ relation because of the large spread affecting the relations from which has been derived.

A different calibration of the SFR in terms of the [OII] luminosity has been obtained by Gallagher et al. (1989) by measuring the [OII] and Hβ fluxes of a variety of blue objects of different types (irregular, amorphous, unclassified galaxies) with a pronounced star formation activity and a relatively low reddening. The numerical constant in their relation is lower than that of Kennicutt's calibration by a factor of 5. It is hard to ascertain to what extent such differences are related to differences in the two samples and to what extent they depend on the adopted approximations. The comparison of Kennicutt's results with those of Gallagher allows to estimate an uncertainty of a factor of 2 or 3 in the evaluation of the SFR.

Line fluxes however are not easily achieved for distant galaxies, for which instead the equivalent widths are measured. It is therefore important to inquire how such quantities can be used to estimate the present SFR. The equivalent width is approximately equal to the ratio of the line flux to the continuum flux at the central wavelength of the line. In the case of the [OII] line we have:

$$EW(OII) \simeq \frac{L(OII)}{F_{\lambda=3727}} \quad (26)$$

and therefore EW(OII) is directly proportional to the present SFR but is also depends on the continuum flux at the central wavelength of the line, which generally is built up with the contribution of all the stars and, which, to a first approximation, is proportional to the luminosity of the nearest photometric band. In the case of the [OII] line this is the U band of the Johnson system. Both $L(OII)$ and $F_{\lambda=3727}$ depend in the same way on the mass of the galaxy and therefore the equivalent width is the same for two galaxies with the same shape of the SFR but different masses. This behaviour is confirmed by a series of models with a wide range of ages and different star formation histories. These models reproduce both normal local morphological types and bursts of different intensity and length in ellipticals and spirals (Sa and Sc).

In Fig. 8, where the equivalent width and the luminosity of the OII line are reproduced, three models are shown with EW = 46 Å and with completely different star formation histories: one point corresponds to an elliptical with burst and the the other two to spirals with different bursts. Models lying on the dashed line on the top of the diagram instead have SFRs with the same shape but differ by the value of M_B which ranges from -18 to -21 mag. Such large spread appears also from the analogous observed diagram of Gallagher et al (1989). It is then confirmed that only the shape of the SFR affects the equivalent width while

the line luminosity depends both on its shape and the mass of the galaxy.

A relation between flux and equivalent width has been obtained directly from the models:

$$\psi = 1.1 \times L_U[EW(OII) + 1.46] \quad (27)$$

where L_U is in units of 10^{42} ergs per second. This relation allows one to derive the mean SFR averaged over the last 10^7 yr from EW(OII) provided that L_U is also known.

From a subsample of 16 galaxies Kennicutt (1992b) derived a mean relation between the L_B luminosity and the equivalent width of the [OII] line:

$$L(OII) \simeq 1.4 \times 10^{29} \cdot L_B \cdot EW(OII) ergs\, s^{-1} \quad (28)$$

where L_B is given in units of $L_{B,\odot}$.

This equation is the analogous of Eq. (26) with the difference that L_B is used instead of L_U. Both relations would have the same field of applicability if L_B and L_U were proportional. A simple relation between the two luminosities exists only for normal morphological types, while it breaks down in the case of starbursts. Therefore Eq. (28) seems to be less general than (26). When a burst is present L_U does not depend in a simple way on the mean SFR over some time period.

The methods of evaluation the star formation rates described in this section have been applied to the normal galaxies of Kennicutt's sample and the results are collected in Table 7.

The values of β have been computed from the observed (U-B) colour index with the calibration of Fig. 6. The mean value of β for each morphological type progressively decreases starting from the ellipticals (1 Gyr^{-1}), S0 (0.43), Sa, Sab (0.28), Sb, Sbc (0.1), Sc (0.055). This result is in agreement with the well-established interpretation of the colour indices and the spectroscopic properties of galaxies along the Hubble sequence and provides the same conclusions reached by Kennicutt et al. (1994) with the analysis of Scalo's b index. Table 7 clearly shows the large spread in β within each Hubble type thus confirming that a close correspondence does not exist between "morphological" and "spectrophotometric" types, as colour indices and spectral features already have shown. For each galaxy from the observed blue magnitude and from the value of β previously derived the values of ψ_o have been computed with the use of Fig. 7. The SFR computed with (19) at the age of 16 Gyr, in $M_\odot$/yr, is shown in column (10), while in column (11) the evaluation of the same quantity is given as derived from the observed [OII] equivalent widths according to (27). The difference in the results obtained with the two methods is of the same order of magnitude as the uncertainties affecting both procedures. The present evaluation of Scalo's b parameter is also shown in column (12).

Kennicutt et al. (1994) also performed an analysis with the aid of a spectrophotometric model of EW(Hα) and some colours of nearby spiral galaxies but their results cannot be compared with the present outcomes due to the different assumptions concerning the age of the galaxies.

With the previous considerations relations have been derived able to estimate the SFR from the Hα and [OII] luminosities for every type of galaxies, normal or starburst. Other methods are restricted only to normal galaxies. It is therefore urgent to derive criteria to diagnose the presence or the absence of bursts. It has been pointed out that very large values of the equivalent width of the Hα line (EW $>$ 50 Å) and the OII line (EW $>$ 50 Å , if also lower than solar metallicities are considered) are typical of starbursts. Also negative Hδ equivalent widths are indicative of a bursts since in late type systems this line is at most emission-filled. On the contrary positive values of EW(Hδ) larger than 3 are indicative of a galaxy which hosted a burst ended 500 - 1000 Myr ago. Therefore the EW(OII)- EW(Hδ) diagram is a valid tool to single out starbursts. With reference to the Fig. 9 normal galaxies are located in a central band with $0 \geq EW(H\delta) \leq 3$ and $EW(OII) \leq 50$ Å. Models with a current burst fall on the left/top of this band; the more intense and of smaller length is the burst, the farthest is its location from the band. Models of the same intensity with increasing length tend to approach the more to the band: this behaviour is selfexplanatory since both line fluxes become saturated, being connected to the number of stars younger than some 10^7 years while the continuum keeps increasing. A consequence of this is that weak bursts and those intense and of large length can get confused with normal galaxies. In Fig. 9 for a current burst the line $\psi_1/\psi_o = const$ is drawn.

Models in the post-burst phase fall in the region on the right of the band of normal systems; the farther they are from it the larger was the number of stars produced by the burst. These post-starburst models assume the star formation stops at the end of the burst and therefore have EW(OII)=0.

Such lines are independent of the type of underlying galaxy, provided that the burst is sufficiently intense: in such situations an estimate of the intensity of the burst is possible. In the diagram the objects of Kennicutt's sample are shown: they confirm the conclusions reached from the analysis of the models. Obviously the same information is provided by the EW(Hα)-EW(Hδ) diagram.

7. Conclusions

The comparison with Kennicutt's spectra has shown that the model nicely reproduces the emission lines of observed spectra, with the exceptions of the OIII line at λ = 5007, as previously discussed.

To a first approximation the relations between the intensities of the emission lines are similar both for normal galaxies and those showing a stronger astrogenetic activity: this is reasonable since all such quantities are only affected by young stars. However peculiar objects present a larger spread, consequence of the variety of the parameters characterizing the bursts.

The analysis performed with the models confirms and extends Kennicutt's conclusions (1992b): the $H\alpha$ and [OII] luminosities are good indicators of the present star formation. The equivalent widths of these lines, which usually are the only available data in the case of distant galaxies, can be also profitably

Table 8.

Age	Sa	Sb	Sc	Sd
0.00E+00	0.60	0.45	0.25	0.10
2.50E+08	1.57	0.98	0.47	0.18
5.00E+08	2.44	1.47	0.69	0.27
7.50E+08	3.16	1.91	0.90	0.36
1.00E+09	3.72	2.28	1.08	0.44
1.25E+09	4.10	2.59	1.25	0.52
1.50E+09	4.27	2.81	1.39	0.59
1.75E+09	4.24	2.95	1.51	0.66
2.00E+09	3.97	3.00	1.60	0.72
2.25E+09	3.61	2.95	1.66	0.78
2.50E+09	3.28	2.80	1.69	0.83
2.75E+09	2.99	2.61	1.68	0.87
3.00E+09	2.73	2.44	1.64	0.90
3.25E+09	2.49	2.28	1.58	0.92
3.50E+09	2.27	2.13	1.52	0.93
3.75E+09	2.07	1.99	1.46	0.94
4.00E+09	1.89	1.86	1.41	0.93
4.25E+09	1.73	1.73	1.35	0.91
4.50E+09	1.58	1.62	1.30	0.90
4.75E+09	1.45	1.52	1.26	0.89
5.00E+09	1.32	1.42	1.21	0.87
5.24E+09	1.21	1.32	1.17	0.86
5.50E+09	1.10	1.24	1.12	0.85
5.75E+09	1.01	1.16	1.08	0.84
6.00E+09	0.92	1.08	1.04	0.82
6.24E+09	0.85	1.01	1.00	0.81
6.50E+09	0.77	0.95	0.97	0.80
6.75E+09	0.71	0.89	0.93	0.79
7.00E+09	0.65	0.83	0.90	0.78
7.24E+09	0.59	0.78	0.87	0.76
7.50E+09	0.54	0.73	0.84	0.75
7.75E+09	0.50	0.68	0.81	0.74
8.00E+09	0.45	0.64	0.78	0.73
8.24E+09	0.42	0.60	0.75	0.72
8.50E+09	0.38	0.56	0.72	0.71
8.75E+09	0.35	0.52	0.69	0.70
9.00E+09	0.32	0.49	0.67	0.69
9.24E+09	0.29	0.46	0.65	0.68
9.50E+09	0.27	0.43	0.62	0.67
9.74E+09	0.24	0.40	0.60	0.66
1.00E+10	0.22	0.37	0.58	0.65
1.02E+10	0.20	0.35	0.56	0.64
1.05E+10	0.19	0.33	0.54	0.63
1.07E+10	0.17	0.31	0.52	0.62

Table 8. (continued)

Age	Sa	Sb	Sc	Sd
1.10E+10	0.16	0.29	0.50	0.61
1.12E+10	0.14	0.27	0.48	0.60
1.15E+10	0.13	0.25	0.46	0.60
1.17E+10	0.12	0.24	0.45	0.59
1.20E+10	0.11	0.22	0.43	0.58
1.22E+10	0.10	0.21	0.42	0.57
1.25E+10	9.57E-02	0.19	0.40	0.56
1.27E+10	8.78E-02	0.18	0.39	0.55
1.30E+10	8.05E-02	0.17	0.37	0.55
1.32E+10	7.38E-02	0.16	0.36	0.54
1.35E+10	6.77E-02	0.15	0.35	0.53
1.37E+10	6.21E-02	0.14	0.33	0.52
1.40E+10	5.70E-02	0.13	0.32	0.52
1.42E+10	5.22E-02	0.12	0.31	0.51
1.45E+10	4.79E-02	0.11	0.30	0.50
1.47E+10	4.39E-02	0.11	0.29	0.49
1.50E+10	4.03E-02	0.10	0.28	0.49
1.52E+10	3.70E-02	9.71E-02	0.27	0.48
1.55E+10	3.39E-02	9.10E-02	0.26	0.47
1.57E+10	3.11E-02	8.53E-02	0.25	0.47
1.60E+10	2.85E-02	7.99E-02	0.24	0.46

Table 9.

Type	<Z>	Z	SFR	M_g/M_{tot}
Sa	1.13×10^{-2}	5.41×10^{-2}	0.03	5.92×10^{-3}
Sb	2.39×10^{-2}	4.01×10^{-2}	0.80	0.02
Sc	1.81×10^{-2}	2.20×10^{-2}	2.45	0.11
Sd	6.13×10^{-3}	8.61×10^{-3}	4.57	0.43

used together with the continuum flux at the line wavelength. This last quantity can be estimated by means of a nearby photometric band: in the case of the [OII] line the nearest one is the U band.

The occurrence of current bursts can be ascertained by means of exceptionally large equivalent widths of H_α, [OII] emission lines, by the presence of the Hδ line in emission and by very small values of the D_{4000} index. A large equivalent width (EW > 3Å) of the Hδ line in absorption is instead indicative of a burst already ended (by about 1-2 Gyr). It must be pointed out however that bursts cannot always be singled out. For instance models of galaxies with a burst with particular values of the parameters can fall in the EW(OII) - EW(Hδ) diagram just in the region filled by normal objects and this happens not only with the weak and short lasting bursts.

The information supported by the (U-B) e (B-V) colours is equivalent to that arising from the emission lines only in the case of normal galaxies. Very blue colour indices also witness current bursts. In the case of normal galaxies the history of star formation can be estimated from photometric data. The (U-B), or another broad band colour index, can be used to evaluate the e-folding time of the star formation process, while M_V, for instance, gives then the initial value of the SFR. The D_{4000} index has been calibrated to yield the ratio of the SFR averaged over the last 5 billion years to the present SFR. If this last quantity is derived from the emission lines, the mean SFR can be estimated.

Attempts to give quantitative estimates of the SF histories in galaxies hosting a burst generally fail, essentially because of the large number of parameters involved.

Acknowledgements. We acknowledge the availability of the Kennicutt's galaxy atlas and the Jacoby et al's stellar library from the NDSS-DCA Astronomical Data Center. B.M.P. acknowledges the receipt of a grant from the Department of Physics of the University of Pisa. This work was supported in part by the Formation and Evolution of Galaxies network set up by the European Commission under contract ERB FMRX-CT96-086 of its TMR programme.

Appendix A

The SFRs of the different Hubble types have been obtained by constraining the spectrophotometric galaxy models with the present day gas fraction, metal content and UBV colours. This work is part of an unpublished Master Degree Thesis (Auddino, University of Padova 1992).

The results for spiral galaxies are shown in Table 8. The first column gives the age in years while the others show the SFR in arbitrary units for each type. Table 9 gives the resulting average and present metallicity, the present SFR (in $M_{\odot}yr^{-1}$ if the galactic mass is $10^{11}M_{\odot}$) and fraction of gaseous mass for an age of 16 Gyr.

References

Aller L.H., 1984, Physics of Thermal Gaseous Nebulae, Kluwer, Dordrecht
Barbaro G., Olivi F.M., 1986, Spectrophotometric Models of Galaxies. In: Chiosi C., Renzini A. (eds.) Spectral Evolution of Galaxies. Reidel, Dordrecht, p. 283
Barbaro G., Olivi F.M., 1989, ApJ 337, 125
Bessell M.S., Brett J.M., 1988, PASP 100, 1134
Binette L., Magris C.G., Stasinska G., Bruzual A.G., 1994, A&A 292, 13
Czyzak S., Keyes C.D., Aller L.H., 1986, ApJS 61, 159
De Vaucoulers G., De Vaucoulers A., Corwin H.G.Jr et al., 1991, Third Reference Catalogue of Bright Galaxies, Springer-Verlag
Dressler A., Gunn J.E., 1982, ApJ 263, 533
Ferland G.J., 1991, Hazy: a brief introduction to Cloudy 80.06, OSU Astronomy Department - Internal Report 91-01
Gallagher J.S., Bushouse H., Hunter D.A.: 1989, AJ 97, 700
Garcia-Vargas M.L., Bressan A., Diaz A.I., 1995, A&AS 112, 13
Jacoby G.H., Hunter D.A., Christian C.A., 1984, ApJS 56, 257
Kennicutt R.C.Jr, 1983, ApJ 272, 54
Kennicutt R.C.Jr, 1992a, ApJS 79, 255
Kennicutt R.C.Jr, 1992b, ApJ 388, 310
Kennicutt R.C.Jr, Tamblyn P., Congdon C.W., 1994, ApJ 435, 22
Koornneef J., 1983, A&A 128, 84
Kurucz R., 1979, ApJS 40, 1
Kurucz R., 1993, CD-Rom n.13, version 22/10/93
Lançon A., Rocca-Volmerange B., 1992, A&AS 96, 593 (LRV)
Landolt–Börnstein, 1982, Numerical Data and Functional Relationships in Science and Technology, Springer-Verlag, vol.2, subvol. b
Mayya Y.D., 1995, AJ 109, 2503
Olofsson K., 1989, A&AS 80, 317
Osterbrock D.E., 1989, Astrophysics of Gaseous Nebulae and Active Galactic Nuclei, University Science Books, Mill Valley, California
Panagia N., 1973, AJ 78, 929
Poggianti B.M., Barbaro G., 1996, A&A , in press
Rubin R.H., 1985, ApJS 57, 349
Sandage A., 1986, A&A 161, 89
Scalo J.M., 1986, Fund. Cos. Phys. 11, 1
Stasinska G., 1990, A&AS 83, 501
Stasinska G., Leitherer C., 1996, ApJS 107,
Zaritsky D., Kennicutt R.C. Jr., Huchra J.P., 1994, ApJ 420, 87

This article was processed by the author using Springer-Verlag LaTeX A&A style file *L-AA* version 3.